Inorganic Chemistry

Article

pubs.acs.org/IC

Flux Synthesis, Structure, Properties, and Theoretical Magnetic Study of Uranium(IV)-Containing $A_2USi_6O_{15}$ (A = K, Rb) with an Intriguing Green-to-Purple, Crystal-to-Crystal Structural Transition in the K Analogue

Gregory Morrison,[†] Harry Ramanantoanina,[‡] Werner Urland,[‡] Mark D. Smith,[†] and Hans-Conrad zur Loye*[,†]

[†]Department of Chemistry and Biochemistry, University of South Carolina, Columbia, South Carolina 29208, United States

[‡]Department of Chemistry, University of Fribourg, Chemin du Musée 9, 1700 Fribourg, Switzerland

Supporting Information

ABSTRACT: The flux growth of uranium(IV) oxides presents several challenges, and to the best of our knowledge, only one example has ever been reported. We succeeded in growing two new reduced uranium silicates $A_2USi_6O_{15}$ (A = K, Rb) under flux growth conditions in sealed copper tubes. The compounds crystallize in a new structure type with space group $C2/c$ and lattice parameters a = 24.2554(8) Å, b = 7.0916(2) Å, c = 17.0588(6) Å, β = 97.0860(6) ° (K) and a = 24.3902(8) Å, b = 7.1650(2) Å, c = 17.2715(6) Å, β = 96.8600(6) ° (Rb). $A_2USi_6O_{15}$ (A = K, Rb) are isocompositional to a previously reported $Cs_2USi_6O_{15}$, and the two structures are compared. $K_2USi_6O_{15}$ undergoes an interesting crystal-to-crystal structural phase transition at $T \approx 225$ K to a triclinic structure, which is accompanied by an intense color change. The magnetic properties of $A_2USi_6O_{15}$ (A = K, Rb, Cs) are reported and differ from the magnetism observed in other U^{4+} compounds. Calculations are performed on the $(UO_6)^{-8}$ clusters of $K_2USi_6O_{15}$ to study the cause of these unique magnetic properties.

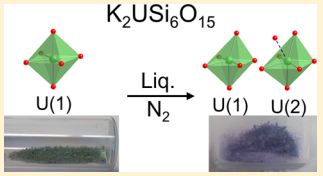

INTRODUCTION

Uranium silicates have been studied as the abundance of silicon in the earth's crust can readily lead to the formation of uranium silicates when spent nuclear fuel interacts with the environment[1,2] or when a reactor core experiences a meltdown.[3] Furthermore, the high melting point and durability of many silicates make uranium silicates good candidates for nuclear waste storage materials. For this application, U(IV)-containing silicates are desired, due to the low solubility of U(IV) ions in water.[4,5] Not surprisingly, the majority of the naturally occurring uranium silicates, formed in an oxygen-rich environment, as well as most laboratory-prepared uranium silicates, contain uranium in the fully oxidized U(VI) oxidation state.[6−14] Nonetheless, several examples of laboratory-prepared U(IV)-containing silicates have been reported, namely, $Cs_2U^{4+}Si_6O_{15}$,[13] $Cs_2K(U^{4+/5+}O)_2Si_4O_{12}$,[15] $Cs_4(U^{5+}O)(U^{4+/5+}O)_2(Si_2O_7)_2$,[16] and $Na_7U^{4+}O_2(U^{5+}O)_2(U^{5+/6+}O_2)_2Si_4O_{16}$.[17] Notably, $Cs_2USi_6O_{15}$ contains $[Si_2O_5]$ unbranched dreier single layers connected into a three-dimensional framework by UO_6 octahedra.[13]

Almost all of the reported uranium(IV)-containing silicates have been grown under hydrothermal conditions, typically with UO_3 and a reducing agent. For example, $Cs_2USi_6O_{15}$ was synthesized through the reduction of UO_3 by Al metal in the presence of CsF and SiO_2 under hydrothermal conditions.[13] An exception is $(Ca_{0.5}Na_{0.5})_2NaUSi_8O_{20}$, which was grown using a flux-assisted solid-state synthesis, in which a small amount of Na_2WO_4 was used to substantially reduce the temperature required for single-crystal growth.[18] Along with hydrothermal growth, the flux growth of reduced uranium oxides is desirable as the higher temperature regime available to flux growth offers the potential of stabilizing new compounds that cannot be grown at lower temperatures. However, the flux growth of uranium(IV)-containing oxides is extremely rare. (Cu,Mn)-UMo_3O_{12} has been prepared via flux growth using $UO_2(CH_3COO)_2{\cdot}2H_2O$ as a uranium source, a MoO_3 flux, and Ar to provide an inert atmosphere,[19] and $K_8U_7O_{24}$ has been grown using a mixture of UO_2 and UO_3 as the uranium source and a KF flux in a sealed copper tube.[20] The flux growth of several U(V) oxides has been reported from Cs_2SO_4,[21] H_3BO_3,[22] and ACl (A = alkali metal) flux.[23] The single-crystal synthesis of several U(IV) fluorides has also been reported using UF_4 and a LiCl−$ZnCl_2$ eutectic flux under argon in a monel alloy reactor.[24,25] Furthermore, the flux growth of many reduced uranium chalcogenides using a variety of fluxes including BaS, $BaBr_2$/KBr, and CsCl, in sealed tubes, has been reported.[26−32] However, the flux synthesis of uranium(IV) oxides presents several further challenges. UO_2 is inert to many solvents, including alkali chloride fluxes[33] such as the one used for the U(IV) fluoride syntheses. Furthermore, the low oxygen concentrations required for the synthesis of reduced uranium oxides often favors the formation of nonoxide products.[34]

Received: March 10, 2015
Published: May 15, 2015

DOI: 10.1021/acs.inorgchem.5b00556
Inorg. Chem. 2015, 54, 5504−5511

Although UO_2 is only weakly soluble in chloride melts,[33] it readily dissolves in the alkali fluoride fluxes that we have explored for the crystal growth of U(VI)-containing oxides.[20] Using this approach, we succeeded in growing single crystals of two new reduced uranium silicates, $A_2USi_6O_{15}$ (A = K, Rb), using the flux growth method. These compounds, while isocompositional to the previously reported $Cs_2USi_6O_{15}$, adopt a new monoclinic structure type. Herein, we report the flux growth of $A_2USi_6O_{15}$ (A = K, Rb, Cs), compare the two structure types, and report the optical and magnetic properties of these three compounds along with a theoretical study of the magnetism of $K_2USi_6O_{15}$.

EXPERIMENTAL SECTION

Synthesis. $A_2USi_6O_{15}$ (A = K, Rb, Cs) were grown using the flux growth method. KF (Alfa Aesar, powder, 99%), KCl (Mallinckrodt Chemicals, crystalline, ACS grade), RbF (Alfa Aesar, crystalline, 99.7%), RbCl (Alfa Aesar, crystalline, 99%), CsF (Strem Chemicals, powder, 99.9%), and CsCl (Alfa Aesar, crystalline, 99%) were used as received. SiO_2 (Aldrich, fused pieces <4 mm, 99.99%) was ground in a ball mill for several hours and passed through a 250 μm sieve. UO_2 was prepared by heating U_3O_8 (International Bio-Analytical Industries, powder, ACS grade) in a tube furnace at 650 °C for 18 h under a flow of 4% H_2 in N_2. ***Caution!*** *Although the uranium precursors used contain depleted uranium, standard safety measures for handling radioactive substance should be followed.*

$A_2USi_6O_{15}$ was prepared by layering a mixture of 0.5 mmol UO_2 and 3 mmol SiO_2 under a mixture of 9 mmol AF and 11 mmol ACl in a copper tube, which was crimped and sealed on one end with a spot-welder. The AF/ACl flux is on the eutectic of KF/KCl (45% KF, 606 °C) and near the eutectics for RbF/RbCl (46.4% RbF, 550 °C) and CsF/CsCl (49.6% CsF, 439 °C). The reagents were dried in a vacuum furnace at 160 °C for 15 min before the other end of the tube was crimped and sealed. The sealed tubes were placed in tube furnaces under flow of nitrogen to prevent the copper from oxidizing and rapidly heated to 900 °C in 1.5 h, dwelled at this temperature for 12 h, and slowly cooled to 700 °C (K), 500 °C (Rb), or 400 °C (Cs) at a rate of 2 °C/h (K) or 6 °C/h (Rb, Cs), at which temperature the furnace was shut off. The different final reaction temperatures were used due to the different melting points of the eutectic or nearly eutectic fluxes. All three compounds could be grown using the 6 °C/h cooling rate, but the 2 °C/h rate yielded larger crystals. This slower cooling rate was important for $K_2USi_6O_{15}$ as crystals of it needed to be picked by hand, vide infra. After heating, the tubes were then cut open, the excess flux was removed with water under sonication, and the resulting products were separated via vacuum filtration and dried with acetone.

For the K reaction, the reaction yielded faint green polyhedral crystals of $K_2USi_6O_{15}$, shown in Figure 1a, as the major product along with an intensely green colored impurity that could not be identified via powder X-ray diffraction. For the Rb reaction, the reaction yielded faint green polyhedral crystals of $Rb_2USi_6O_{15}$, shown in Figure 1b, along with a large amount of polycrystalline $Rb_2(SiF_6)$. For the Cs reaction, the synthesis yielded phase-pure polycrystalline $Cs_2USi_6O_{15}$.

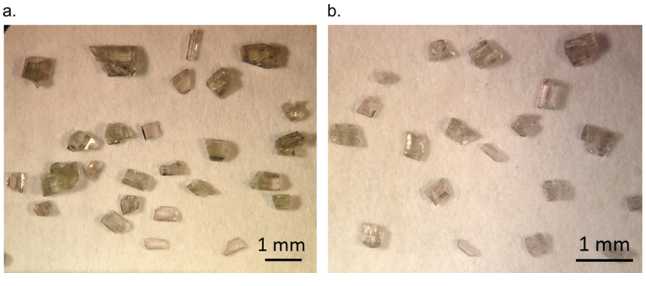

Figure 1. Single crystals of (a) $K_2USi_6O_{15}$ and (b) $Rb_2USi_6O_{15}$.

The flux-grown $Cs_2USi_6O_{15}$ adopts the same structure as the previously reported, hydrothermally grown, $Cs_2USi_6O_{15}$. On the basis of uranium, the percent yield of the reactions are 61% (K), 29% (Rb), and 37% (Cs). Phase-pure samples of the K and Rb analogues were obtained by picking crystals (K) or sieving the sample (Rb). Powder diffraction patterns of all three phase pure samples are shown in Supporting Information Figure S1.

Structure. Structure determination for $A_2USi_6O_{15}$ (A = K, Rb) was performed via single-crystal X-ray diffraction. Data were collected on a Bruker SMART APEX CCD diffractometer with a Mo Kα source (λ = 0.710 73 Å). Data collection and unit cell determination were performed using SMART,[35] data integration was performed using SAINT+,[36] and absorption correction was applied using SADABS.[37] An initial structural solution was obtained using direct methods[38] and refined with SHELXL-2014[38] using the ShelXe interface.[39] The final structural solutions were checked with the ADDSYM operation in the PLATON suite,[40] which found no evidence for higher symmetry. Crystallographic data are provided in Table 1. Phase purity of samples used for physical properties measurements was checked using powder X-ray diffraction. Data were collected on a Rigaku Ultima IV diffractometer with a Cu Kα source (λ = 1.540 56 Å) and a scintillation counter. Energy-dispersive X-ray spectroscopy, EDS, was performed on single crystals of $A_2USi_6O_{15}$ (A = K, Rb) using a TESCAN Vega-3 SBU equipped with an EDS detector. EDS data confirmed the presence of A, U, Si, and O and found no evidence of any F or Cl being present in the crystals, despite being present in the flux.

Table 1. Crystallographic Data for $A_2USi_6O_{15}$ (A = K, Rb)

formula	$K_2USi_6O_{15}$	$K_2USi_6O_{15}$	$Rb_2USi_6O_{15}$
space group	$C2/c$	$P\bar{1}$	$C2/c$
a (Å)	24.2554(8)	7.2196(5)	24.3902(8)
b (Å)	7.0916(2)	12.0518(8)	7.1650(2)
c (Å)	17.0588(6)	17.1967(12)	17.2715(6)
α (deg)	90	99.514(2)	90
β (deg)	97.0860(6)	91.002(2)	96.8600(6)
γ (deg)	90	106.116(2)	90
V (Å^3)	2911.86(16)	1414.52(17)	2996.69(17)
Z	8	4	8
crystal dimensions (mm^3)	0.20 × 0.10 × 0.05	0.12 × 0.10 × 0.08	0.16 × 0.14 × 0.14
temperature (K)	295(1)	100(2)	295(1)
density (g cm^{-3})	3.306	3.403	3.624
q range (deg)	1.69−28.28	1.20−35.03	1.68−28.30
μ (mm^{-1})	12.294	12.654	17.846
data collection and refinement			
collected reflections	19 361	43 979	22 618
unique reflections	3627	11 604	3715
R_{int}	0.0293	0.0350	0.0309
h	$-32 \le h \le 32$	$-11 \le h \le 10$	$-32 \le h \le 32$
k	$-9 \le k \le 9$	$-18 \le k \le 18$	$-9 \le k \le 9$
l	$-22 \le l \le 22$	$-27 \le l \le 27$	$-22 \le l \le 23$
$\Delta\rho_{max}$ (e Å^{-3})	0.676	2.894	1.573
$\Delta\rho_{min}$ (e Å^{-3})	−0.634	−1.233	−1.372
GOF	1.034	1.047	1.088
extinction coefficient	0.000 162(13)		0.000 417(15)
[a] $R_1(F)$ for $F_o^2 > 2\sigma(F_o^2)$	0.0259	0.0294	0.0355
[b] $R_w(F_o^2)$	0.0574	0.0624	0.0751

[a] $R_1 = \sum||F_0| - |F_c||/\sum|F_0|$ [b] $wR_2 = [\sum w(F_o^2 - F_c^2)^2/\sum w(F_0^2)^2]^{1/2}$; $P = (F_o^2 + 2F_c^2)/3$; $w = 1/[\sigma^2(F_o^2) + (0.0000P)^2 + 80.0P]$ for K analogue (295 K); $w = 1/[\sigma^2(F_o^2) + (0.0267P)^2 + 2.8824P]$ for K analogue (100 K); $w = 1/[\sigma^2(F_o^2) + (0.0000P)^2 + 165.0P]$ for Rb analogue

DOI: 10.1021/acs.inorgchem.5b00556
Inorg. Chem. 2015, 54, 5504−5511

Physical Properties. UV−vis diffuse reflectance was collected on a PerkinElmer Lambda 35 UV−vis scanning spectrophotometer equipped with an integrating sphere. Data were collected for the range of 200−900 nm and converted to absorbance using the Kubelka−Munk equation.[41]

Magnetic properties were measured on a Quantum Design MPMS 3 SQUID magnetometer. Samples of ground single crystals of $A_2USi_6O_{15}$ (A = K, Rb, Cs) were massed on a balance sensitive to 0.01 mg and loaded into vibrating sample magnetometer (VSM) powder holders. Magnetic susceptibility was collected under zero-field-cooled conditions from 2 to 300 K with H = 1000 Oe using the direct-current (DC) scan mode. The magnetic moment was corrected for shape and radial offset effects by comparing the moment measured at 30 K with DC and VSM scan modes, as demonstrated by Morrison et al.[42] A second, smaller sample of unground single crystals (K) or a pellet of pressed powder (Rb, Cs) was mounted on an oven stick, and the susceptibility was measured from 300 to 700 K with H = 1000 Oe using the QD oven option for the MPMS 3 in DC scan mode. Because of the small sample size and odd shape, the absolute susceptibility was determined by normalizing the 300 K susceptibility to the 300 K susceptibility from the VSM powder holder measurement.

Theoretical Studies. The magnetic properties of the low- and high-temperature $K_2USi_6O_{15}$ phases were studied theoretically by ligand field density functional theory (LFDFT)[43] modeling of $(UO_6)^{-8}$. Point charges were added to neutralize the high negative charge of the cluster, mimicking well the local and long-range environment of the U^{4+} center. The DFT calculations were performed using the Amsterdam Density Functional (ADF2013.01) program package,[44] under the so-called Average of Configuration (AOC) type calculation.[45] A hybrid B3LYP functional[46] was used to represent the exchange-correlation energy and potential. The molecular orbitals were expanded using triple-ζ plus one polarization STO function (TZP) for the U and the O atoms. The structure of $(UO_6)^{-8}$ was extracted from the crystal structure of $K_2USi_6O_{15}$, and no reconsideration of the structure by geometry optimization is performed.

RESULTS AND DISCUSSION

Synthesis. The flux growth of reduced uranium oxides poses three main challenges. First, the reaction must be devoid of oxygen. Previously, this has been accomplished in the flux growth of reduced oxides by heating the reaction under vacuum,[47] under inert atmosphere,[48] or in a sealed vessel.[49] In our reactions, we accomplished this by sealing the reactants in a copper tube. The copper tube was then placed in a tube furnace under N_2 flow to prevent the copper tube from oxidizing on the outside and degrading during the course of crystal growth.

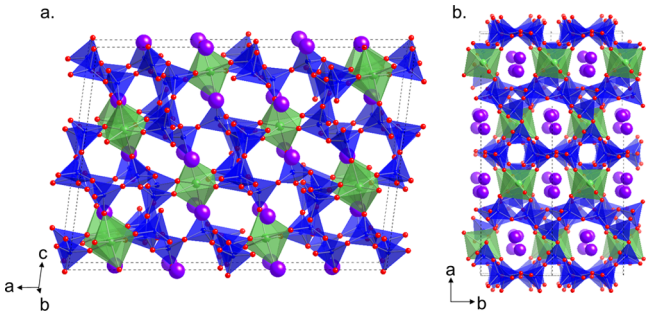

Figure 2. Room-temperature structure of $K_2USi_6O_{15}$ showing (a) the three-dimensional connectivity of the uranium and silicon polyhedra and (b) the c-direction highlighting the channels in the framework. Uranium atoms are shown in green, silicon in blue, potassium in purple, and oxygen in red.

Table 2. Select Interatomic Distances for $A_2USi_6O_{15}$ (A = K, Rb, Cs) (Å) at Room Temperature

interaction	$K_2USi_6O_{15}$	$Rb_2USi_6O_{15}$	interaction	$Cs_2USi_6O_{15}$[13]
U−O(14)	2.207(4)	2.217(6)	U−O(1)	2.209(7)
U−O(9)	2.232(4)	2.226(5)	U−O(7) × 2	2.236(5)
U−O(11)	2.235(4)	2.233(5)	U−O(10)	2.254(7)
U−O(1)	2.259(4)	2.262(5)	U−O(4) × 2	2.257 (4)
U−O(6)	2.266(4)	2.264(5)		
U−O(8)	2.284(4)	2.279(5)		

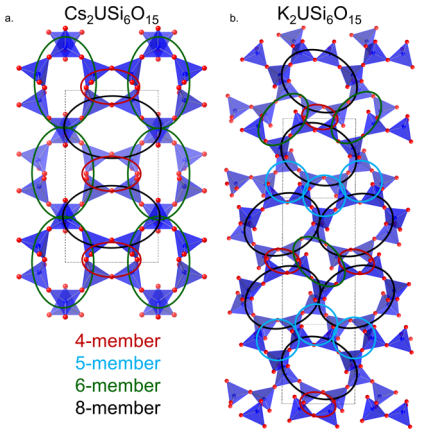

Figure 3. Silicate slabs in (a) $Cs_2USi_6O_{15}$ and (b) $K_2USi_6O_{15}$. The silicate rings are color-coded to highlight the relationship between the two slabs, see legend. The silicate slabs lie in the (0 1 0) plane (Cs) and ($\bar{1}$ 0 1) plane (K).

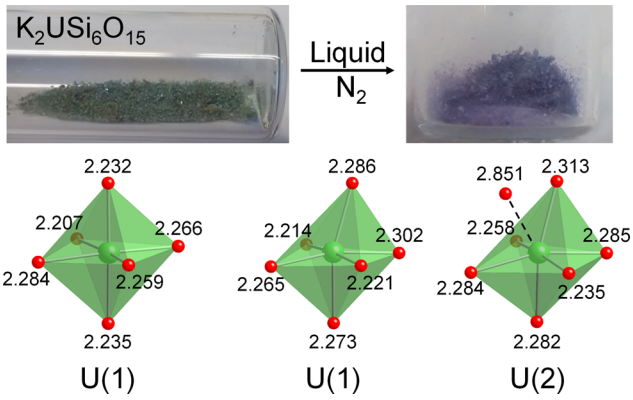

Figure 4. Bulk crystals of $K_2USi_6O_{15}$ at room and liquid nitrogen temperatures. The uranium environments and U−O interatomic distances (Å) at the two temperatures are shown below.

The second challenge in the flux growth of reduced uranium oxides is that UO_2 is insoluble in many fluxes. For example, UO_3 and U_3O_8 readily dissolve in ACl fluxes (A = alkali metal),[50] whereas UO_2 is inert in these fluxes. UO_2 is soluble in AF and AF/MoO_3 (A = alkali metal) mixed fluxes; however, reactions using either of these fluxes only produced fluoride products. This is the third challenge in the flux growth of reduced uranium oxides, namely, that the low oxygen concentration of the reactions often produce nonoxide products. This has previously been observed in the synthesis of uranyl oxychlorides, where open systems form oxide products and sealed systems form oxychlorides.[34] This problem was mediated by using a mixed AF/ACl flux (45 atomic % AF). By diluting the reactive fluoride with the unreactive chloride, we

DOI: 10.1021/acs.inorgchem.5b00556
Inorg. Chem. 2015, 54, 5504−5511

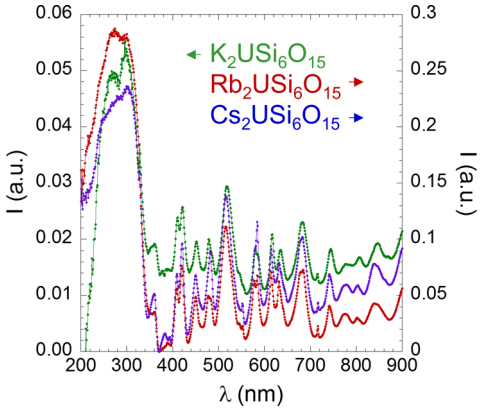

Figure 5. UV−vis absorbance spectra of $A_2USi_6O_{15}$ (A = K, Rb, Cs).

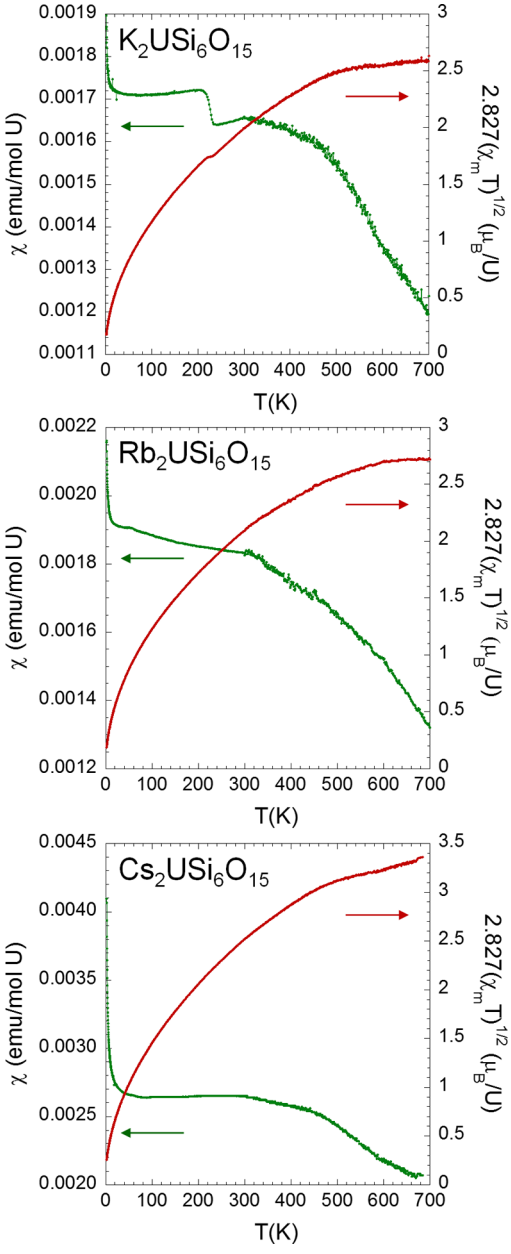

Figure 6. Magnetic susceptibility and $2.827(\chi_m T)^{1/2}$ for $A_2USi_6O_{15}$ (A = K, Rb, Cs).

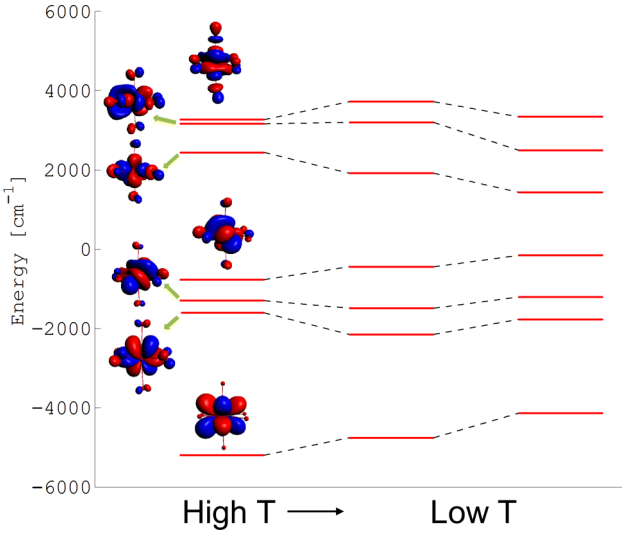

Figure 7. Representation of the energies of the frontier Kohn−Sham orbitals of $(UO_6)^{-8}$ obtained from the output of AOC-type calculation. The three diagrams represent the cases of the structure belonging to the high-temperature U site (left) and the low-temperature U(1) site (middle) and U(2) site (right) of $K_2USi_6O_{15}$.

successfully maintained the UO_2 solubility while preventing the formation of fluoride products.

Structure. $A_2USi_6O_{15}$ (A = K, Rb) are members of a new structure type, which crystallizes in the monoclinic space group $C2/c$ with lattice parameters a = 24.2554(8) Å, b = 7.0916(2) Å, c = 17.0588(6) Å, and β = 97.0860(6)° (K) and a = 24.3902(8) Å, b = 7.1650(2) Å, c = 17.2715(6) Å, and β = 96.8600(6)° (Rb). The structure consists of two unique A sites, one unique U site, six unique Si sites, and 15 unique O sites. All atoms are on general crystallographic positions (Wyckoff site 8*f*, site symmetry 1). Each Si atom is tetrahedrally surrounded by O atoms with bond distances of 1.573(4)−1.640(4) Å (K) and 1.577(6)−1.650(5) Å (Rb), which are typical of silicates.[51] As shown in Figure 2a, the Si tetrahedra corner share to form slabs in the $(\bar{1}01)$ direction. The U atoms are surrounded by six O atoms in an octahedral environment with bond distances, listed in Table 2, of 2.207(4)−2.284(4) Å (K) and 2.217(6)−2.279(5) Å (Rb). These distances are in agreement with the 2.24 Å predicted by Shannon[52] and the U(IV)−O distances observed for other U(IV)-containing silicates.[13,17] Bond valence sum calculations[53,54] yield a U valence of +4.12 for each analogue, in good agreement with the U(IV) obtained from charge balancing. The UO_6 octahedra are isolated from each other and lie in between two silicate slabs, corner sharing with three silicon tetrahedra of each slab. The SiO_4 and UO_6 polyhedra are arranged such that they form channels in the c direction, shown in Figure 2b, in which the A cations are located.

$Cs_2USi_6O_{15}$ was previously reported[13] and crystallizes in a different structure with orthorhombic space group $Cmc2_1$ and lattice parameters a = 7.2717(3) Å, b = 16.3061(7) Å, and c = 13.4983(6) Å.[13] While crystallizing in different structure types, $A_2USi_6O_{15}$ (A = K, Rb) and $Cs_2USi_6O_{15}$ are structurally related. Like the K and Rb structures, the Cs analogue contains slabs of corner-sharing SiO_4 tetrahedra in the (010) direction. Figure 3 shows a perpendicular view of the $Cs_2USi_6O_{15}$ and $K_2USi_6O_{15}$ silicate slabs. The slabs in $Cs_2USi_6O_{15}$ consist of rows of six-member silicate rings in one direction and rows of eight-

DOI: 10.1021/acs.inorgchem.5b00556
Inorg. Chem. 2015, 54, 5504−5511

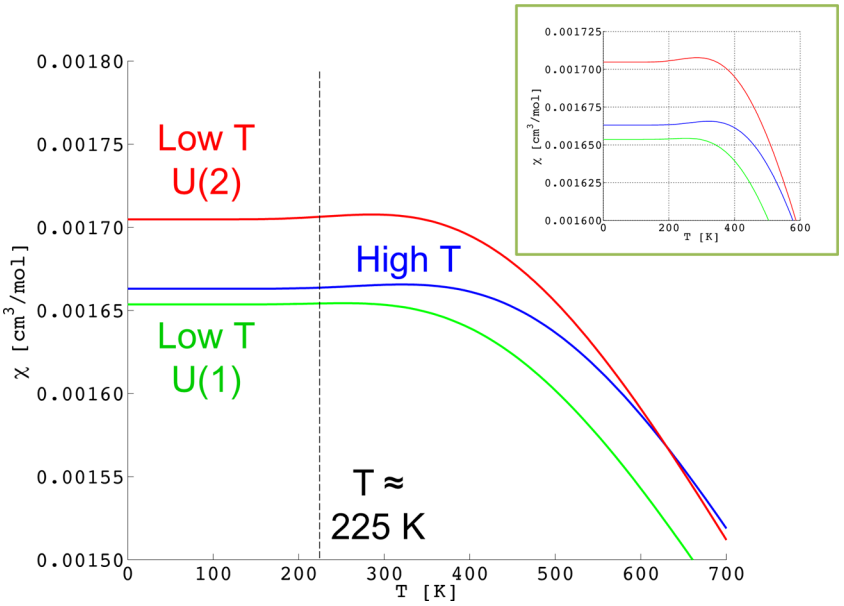

Figure 8. Calculated magnetic susceptibility obtained for $(UO_6)^{-8}$ from the structure belonging to the high-temperature U site (in blue) and the low-temperature U(1) site (in green) and U(2) site (in red) of $K_2USi_6O_{15}$. Calculated Slater−Condon parameters and spin−orbit coupling constant are (in cm^{-1}): F_2 = 225.71, F_4 = 29.83, F_6 = 3.21 and ζ = 2013.9. (inset) The magnified sequence emphasizing the upturn with increasing temperature before the downturn in the susceptibility.

member silicate rings in the perpendicular direction. At the center of every set of two six-member and two eight-member rings is a four-member ring. The silicate slabs of $K_2USi_6O_{15}$ are similar, with perpendicular sets of six- and eight-member rings combining to form four-member rings. However, these sets of rings extend infinitely in one direction forming rows that are separated by rows of five-member rings and rotated by 180° from the rows on either side. In $K_2USi_6O_{15}$, the silicate slabs stack, separated by UO_6 octahedra, such that each successive eight-member ring is on top of the other eight-member rings, creating channels in which the K ions lie. In $Cs_2USi_6O_{15}$, the slabs stack such that a four-member ring of one layer sits directly above the eight-member ring of the previous layer, and therefore, no channels are present.

The K and Rb analogues likely adopt a different structure from the Cs analogue due to the large differences in ionic radii between the three alkali cations.[52] The shortest A−O interactions within the channels of the $A_2USi_6O_{15}$ (A = K, Rb) are 2.754(4) Å (K) and 2.899(5) Å (Rb), which are much smaller than the shortest Cs−O interactions in $Cs_2USi_6O_{15}$, 3.173(3) Å. It is likely that the channels in the rigid three-dimensional uranium silicate framework of the K and Rb structure can not accommodate the much larger Cs cation.[13] It is not unusual for the K and Cs analogues of an isocompositional series to adopt different structure types.[55−59]

Along with the isocompositional compounds $A_2USi_6O_{15}$ (A = K, Rb) and $Cs_2USi_6O_{15}$, there is also a related series of $A_xBSi_6O_{15}$ (A = alkali metal, B = +3 or +4 cation, x = 2 or 3) compounds that contain the same four-, six- and eight-member ring structural motif and adopt a variety of structure types. For example, $Cs_3EuSi_6O_{15}$ contains a three-dimensional silicate framework composed of the motif and $K_3NdSi_6O_{15}$ and $K_2TiSi_6O_{15}$ contain two-dimensional sheets of the motif.[60,61]

Structural Transition. At low temperatures, $K_2USi_6O_{15}$ undergoes a structural transition from the monoclinic $C2/c$ structure to a triclinic structure. This low-temperature phase adopts the $P\bar{1}$ space group with lattice parameters a = 7.2196(5) Å, b = 12.0518(8) Å, c = 17.1967(12) Å, α = 99.514(2)°, β = 91.002(2)°, and γ = 106.116(2)°, which is a distortion of the reduced cell of the high-temperature structure. As expected for a reversible, crystal-to-crystal transition that preserves the single crystalline nature of the sample, the low-temperature structure and silicate sheets, shown in Supporting Information Figures S2 and S3, respectively, look very similar to the high-temperature phase. The reduction to triclinic symmetry doubles the number of all atomic sites, while retaining the site symmetry of 1 (Wyckoff site 2i in $P\bar{1}$). For the uranium centers, shown in Figure 4, the reduced symmetry is associated with a further distortion of UO_6 octahedra. In an ideal octahedron, all six bond lengths l should be the same, and all 12 bond angles ∠ should be 90° leading to standard deviations σ of zero. At 295 K, the uranium site has l = 2.207−2.284 Å (σl = 0.028 Å) and ∠ = 79.394−98.660° ($\sigma\angle$ = 4.87°). At 100 K, U(1) has l = 2.214−2.302 Å (σl = 0.035 Å) and ∠ = 77.762−114.065° ($\sigma\angle$ = 9.07°) and U(2) has l = 2.235−2.313 Å (σl = 0.027 Å) and ∠ = 77.061−119.462° ($\sigma\angle$ = 11.52°). Despite the increased distortion, the bond valence sums remain similar, going from +4.12 at 295 K to +4.02 (U1) and +4.11 (U2) at 100 K, and indicate that the high-temperature U−O bonds are slightly contracted compared to the low-temperature bonds.

Associated with the structural transition are two transitions in the physical properties of $K_2USi_6O_{15}$. First, a jump in the magnetic moment of ground single crystals is observed at $T \approx$ 225 K when cooled, vide infra. The jump in magnetism indicates that the electronic structure of $K_2USi_6O_{15}$ changes significantly as a result of the structural transition. Second, an optical transition occurs with the high-temperature phase being a faint green color and the low-temperature phase having an intense purple color, see Figure 4. This color change indicates that the dominant absorption at high temperature is in the red and shifts to yellow at low temperatures, indicating an increase in the absorption energy. Interestingly, the purple color of the low-temperature phase is typically only observed in U(III)

DOI: 10.1021/acs.inorgchem.5b00556
Inorg. Chem. 2015, 54, 5504−5511

materials.[62] However, bond valence calculations indicate the uranium remains in the tetravalent state at low temperatures.

The color change offers a simplistic method of studying the structural transition. In polycrystalline samples, the transition occurs at $T \approx 225$ K, from magnetism data, and occurs universally, as indicated by a complete color change. When warmed, the crystals rapidly revert to their initial green color. In single crystals, the phase transition is not universal. Single-crystal X-ray analysis of nine crystals found that, when cooled, three of them underwent a transition to the triclinic cell, while the remainder did not. In accordance with this, the three crystals became purple, while the rest exhibited no color change. Furthermore, while in the polycrystalline sample the transition seems to occur sharply at 225 K, in single crystals the transition temperature seems to be lower, with one crystal changing colors at 143(2) K when cooled and at 205(5) K when warmed. It is possible that the high-temperature phase can be supercooled in some cases, which has been observed in some other compounds such as K_2MBr_4 (M = Co, Zn).[63,64] The occurrence of the transition does not appear to be cooling rate or crystal morphology dependent. In all cases, the monoclinic high-temperature phase is obtained when warmed. Despite the same high-temperature structure, no similar transition is observed in $Rb_2USi_6O_{15}$ based on magnetic measurements and the absence of a color change when cooled to 77 K.

Ion Exchange. To investigate the mobility of the alkali cations within the channels of $A_2USi_6O_{15}$ (A = K, Rb), a sample of $K_2USi_6O_{15}$ crystals of suitable size for single-crystal X-ray diffraction was refluxed ($T \approx 140$ °C) in a saturated NaCl solution for 6 h, based on a reported procedure.[65] Diffraction data were then collected on one of the crystals. Both alkali cation sites refined to full occupancy of K, indicating that no K ions migrated to other locations in the channels or were replaced by Na ions. This suggests that the K ions are not mobile within the channels.

Physical Properties. Figure 5 shows the UV−vis absorbance spectra for $A_2USi_6O_{15}$ (A = K, Rb, Cs). All three spectra are very similar and are typical of U(IV)-containing compounds, with a series of sharp, weak absorbance bands above 400 nm due to f−f transitions of the $5f^2$ electrons. The almost identical features of these spectra indicate that in all three compounds, the U atoms have very similar crystalline electric fields. This is expected as, despite the different alkali cations and structure types, all three have similar U environments. At ∼300 nm, each compound has a strong absorption band due to their band gap. The calculated band gaps are 3.58 eV (K), 3.51 eV (Rb), and 3.59 eV (Cs), indicating that all compounds are insulators.

Figure 6 shows the magnetic susceptibilities of $A_2USi_6O_{15}$ (A = K, Rb, Cs). Excluding what is believed to be a Curie tail at low temperatures, all three susceptibilities are nearly temperature-independent up to ∼450 K, at which temperature there is a strong downturn in the susceptibilities. At ∼225 K, the magnetic susceptibility of $K_2USi_6O_{15}$ undergoes a sharp jump with decreasing temperature due to the structural transition. Because of the non-Curie−Weiss behavior, the effective moments were determined using $\mu_{eff} = 2.827(\chi T)^{1/2}$. The moments at 300 K were found to be 2.00 (K), 2.10 (Rb), and 2.52(Cs) μ_B/U, which are in the lower range of the typically observed room-temperature U^{4+} moments, 1.8−3.8 μ_B/U.[66] It is not until between 500 and 600 K that the maximum moments 2.6 (K), 2.7 (Rb), and 3.3 (Cs) are observed. The effective moments observed in $K_2USi_6O_{15}$ and $Rb_2USi_6O_{15}$ are very similar, which is expected as the two crystallize in the same structure. $Cs_2USi_6O_{15}$, which has a higher symmetry U^{4+} environment, shows similar qualitative magnetism, but the observed moment is higher than the other two isocompositional compounds.

The magnetic susceptibility of $A_2USi_6O_{15}$ differs from what is typically observed in the more extensively magnetically studied U(IV) fluorides,[67,68] which typically display Curie−Weiss behavior down to 25−100 K, at which temperature they enter a singlet ground state. There are two factors that may account for the difference between the magnetism of the titled uranium silicates and the previously studied uranium fluorides. First, the uranium environments within the previously studied uranium fluorides are higher coordination and typically higher symmetry than the six-coordinate uranium sites within the current silicates, which have a site symmetry of 1. Second, O^{2-} is a stronger field ligand than F^- potentially leading to larger crystalline electric field splitting energies.[69]

Theoretical Studies. To understand the magnetic behavior in $A_2USi_6O_{15}$, which is different from that observed in other U(IV)-containing compounds, LFDFT calculations were performed on the $(UO_6)^{-8}$ clusters found in the high- and low-temperature structures of $K_2USi_6O_{15}$ (see Figure 4). Figure 7 shows the ligand field energies of the 5f orbitals of U^{4+} as a function of the high- or the two low-temperature U^{4+} sites of $K_2USi_6O_{15}$. The ligand field potential[70] is given in the Supporting Information (Table S1), as well as the calculated multiplet energy levels arising from the $5f^2$ electron configuration of U^{4+} in $(UO_6)^{-8}$ (Figure S4). The ligand field energy spacing is larger in the high-temperature structure because of the shorter U−O bond lengths obtained from the crystal structure consideration. Magnetic susceptibility curves[71] (Figure 8) were calculated for both the high- and low-temperature structures of $K_2USi_6O_{15}$, where a good agreement with the measured magnetic susceptibility in $K_2USi_6O_{15}$ is observed, the susceptibility being temperature-independent at low temperatures, followed by an upturn with increasing temperature before a strong downturn in the susceptibility at ∼450 K.

CONCLUSIONS

Single crystals of uranium(IV)-containing $A_2USi_6O_{15}$ (A = K, Rb) have been grown using the flux growth method. The reactions were performed in sealed copper tubes using UO_2 as a reduced uranium source. An AF flux was used to solubilize the UO_2 but was diluted with ACl (45% AF in ACl) to avoid the formation of uranium fluoride products. The elevated temperature regime available to flux growth compared to other single-crystal growth methods offers the potential to discover new, high-temperature stabilized phases.

$A_2USi_6O_{15}$ (A = K, Rb) crystallizes in a new structure type that is related to the $Cs_2USi_6O_{15}$ structure type and other $A_xBSi_6O_{15}$ (A = alkali metal, B = +3 or +4 cation, x = 2 or 3) structure types. $K_2USi_6O_{15}$ undergoes an interesting crystal-to-crystal phase transition at $T \approx 225$ K, which is associated with a jump in the magnetic susceptibility and an intense color change, indicating a significant altering of the electronic structure. Room-temperature UV−vis absorption data indicate that all $A_2USi_6O_{15}$ (A = K, Rb, Cs) are insulators with similar bandgaps of ∼3.55 eV and similar crystalline electric fields surrounding the U atoms. The magnetic properties of $A_2USi_6O_{15}$ (A = K, Rb, Cs) differ from the magnetism

DOI: 10.1021/acs.inorgchem.5b00556
Inorg. Chem. 2015, 54, 5504−5511

observed in other U^{4+} compounds. Calculations performed on the $(UO_6)^{-8}$ cluster of $K_2USi_6O_{15}$ are in good agreement with the observed magnetism, indicating that the unique magnetism arises due to the local uranium environment.

■ ASSOCIATED CONTENT

Supporting Information

Calculated ligand field potentials for $(UO_6)^{-8}$, powder diffraction patterns, low-temperature $K_2USi_6O_{15}$ figures, and calculated LFDFT multiplet energy levels for $(UO_6)^{-8}$. Single-crystal X-ray diffraction CIFs for $K_2USi_6O_{15}$ (T = 295 and 100 K) and $Rb_2USi_6O_{15}$ (T = 295 K). The Supporting Information is available free of charge on the ACS Publications website at DOI: 10.1021/acs.inorgchem.5b00556.

■ AUTHOR INFORMATION

Corresponding Author

*E-mail: zurLoye@mailbox.sc.edu. Phone: (803) 777-6916. Fax: (803) 777-8508.

Notes

The authors declare no competing financial interest.

■ ACKNOWLEDGMENTS

The experimental work was performed at the Univ. of South Carolina and was supported by the U.S. Department of Energy, Office of Basic Energy Sciences, Division of Materials Sciences and Engineering under Award No. DE-SC0008664. H.R. and W.U. are indebted to the support from the Swiss National Science Foundation and the Swiss State Secretariat for Innovation and Research, which supported the theoretical work.

■ REFERENCES

(1) Wronkiewicz, D. J.; Bates, J. K.; Wolf, S. F.; Buck, E. C. *J. Nucl. Mater.* **1996**, *238*, 78−95.
(2) Burns, P. C.; Olson, R. A.; Finch, R. J.; Hanchar, J. M.; Thibault, Y. *J. Nucl. Mater.* **2000**, *278*, 290−300.
(3) Burns, P. C.; Ewing, R. C.; Navrotsky, A. *Science* **2012**, *335*, 1184−1188.
(4) Finneran, K. T.; Housewright, M. E.; Lovley, D. R. *Environ. Microbiol.* **2002**, *4*, 510−516.
(5) Neck, V.; Kim, J. I. *Radiochim. Acta* **2001**, *89*, 1−16.
(6) Plaisier, J. R.; Ijdo, D. J. W.; de Mello Donega, C.; Blasse, G. *Chem. Mater.* **1995**, *7*, 738−743.
(7) Lee, C.-S.; Wang, S.-L.; Lii, K.-H. *Chem. J. Chin. Univ.* **2011**, *32*, 605−608.
(8) Shashkin, D. P.; Lur'e, E. A.; Belov, N. V. *Kristallografiya* **1974**, *19*, 958−963.
(9) Lee, C.-S.; Wang, S.-L.; Chen, Y.-H.; Lii, K.-H. *Inorg. Chem.* **2009**, *48*, 8357−8361.
(10) Chen, C.-S.; Chiang, R.-K.; Kao, H.-M.; Lii, K.-H. *Inorg. Chem.* **2005**, *44*, 3914−3918.
(11) Huang, J.; Wang, X.; Jacobson, A. J. *J. Mater. Chem.* **2003**, *13*, 191−196.
(12) Liu, H.-K.; Chang, W.-J.; Lii, K.-H. *Inorg. Chem.* **2011**, *50*, 11773−11776.
(13) Liu, H.-K.; Lii, K.-H. *Inorg. Chem.* **2011**, *50*, 5870−5872.
(14) Chen, C.-S.; Kao, H.-M.; Lii, K.-H. *Inorg. Chem.* **2005**, *44*, 935−940.
(15) Lee, C.-S.; Wang, S.-L.; Lii, K.-H. *J. Am. Chem. Soc.* **2009**, *131*, 15116−15117.
(16) Chen, C.-L.; Nguyen, Q. B.; Chen, C.-S.; Lii, K.-H. *Inorg. Chem.* **2012**, *51*, 7463−7465.
(17) Lee, C.-S.; Lin, C.-H.; Wang, S.-L.; Lii, K.-H. *Angew. Chem., Int. Ed.* **2010**, *49*, 4254−4256.
(18) Jin, G. B.; Soderholm, L. *J. Solid State Chem.* **2015**, *221*, 405−410.
(19) Sedello, O.; Mueller-Buschbaum, H. *Z. Naturforsch.* **1996**, *51*, 450−452.
(20) Read, C.; Smith, M.; zur Loye, H.-C. *J. Chem. Crystallogr.* **2014**, *44*, 604−608.
(21) van Egmond, A. B. *J. Inorg. Nucl. Chem.* **1975**, *37*, 1929−1931.
(22) Chevalier, R.; Gasperin, M. *C. R. Acad. Sci. C* **1969**, *268*, 1426−1428.
(23) Read, C. M.; Smith, M. D.; zur Loye, H.-C. *Solid State Sci.* **2014**, *37*, 136−143.
(24) Cousson, A.; Pages, M.; Cousseins, J. C.; Vedrine, A. *J. Cryst. Growth* **1977**, *40*, 157−160.
(25) Cousson, A.; Tabuteau, A.; Pages, M.; Gasperin, M. *Acta Crystallogr., Sect. B* **1979**, *35*, 1198−1200.
(26) Mesbah, A.; Ibers, J. A. *J. Solid State Chem.* **2013**, *199*, 253−257.
(27) Mesbah, A.; Malliakas, C. D.; Lebègue, S.; Sarjeant, A. A.; Stojko, W.; Koscielski, L. A.; Ibers, J. A. *Inorg. Chem.* **2014**, *53*, 2899−2903.
(28) Bugaris, D. E.; Ibers, J. A. *Inorg. Chem.* **2012**, *51*, 661−666.
(29) Ward, M. D.; Oh, G. N.; Mesbah, A.; Lee, M.; Sang Choi, E.; Ibers, J. A. *J. Solid State Chem.* **2015**, *228*, 14−19.
(30) Prakash, J.; Tarasenko, M. S.; Mesbah, A.; Lebègue, S.; Malliakas, C. D.; Ibers, J. A. *Inorg. Chem.* **2014**, *53*, 11626−11632.
(31) Ward, M. D.; Ibers, J. A. *Acta Crystallogr., Sect. E* **2014**, *70*, i4−i4.
(32) Mesbah, A.; Oh, G. N.; Bellott, B. J.; Ibers, J. A. *Solid State Sci.* **2013**, *18*, 110−113.
(33) Blander, M.; Nagy, Z. *Z. Naturforsch., A* **1983**, *38*, 116−119.
(34) Read, C. M.; Yeon, J.; Smith, M. D.; zur Loye, H.-C. *CrystEngComm* **2014**, *16*, 7259−7267.
(35) *SMART*, 5.625; Bruker Analytical X-ray Systems: Madison, WI, 2001.
(36) *SAINT+*, 6.0; Bruker Analytical X-ray Systems: Madison, WI, 2000.
(37) *SADABS*, 2.03; Bruker Analytical X-ray Systems: Madison, WI, 2002.
(38) Sheldrick, G. M. *Acta Crystallogr., Sect. A* **2008**, *64*, 112−122.
(39) Hubschle, C. B.; Sheldrick, G. M.; Dittrich, B. *J. Appl. Crystallogr.* **2011**, *44*, 1281−1284.
(40) Spek, A. L. *Acta Crystallogr., Sect. A* **1990**, *46*, C34.
(41) Kubelka, P.; Munk, F. Z. *Technol. Phys.* **1931**, *12*, 593−601.
(42) Morrison, G.; zur Loye, H.-C. *J. Solid State Chem.* **2015**, *221*, 334−337.
(43) Ramanantoanina, H.; Urland, W.; Cimpoesu, F.; Daul, C. *Phys. Chem. Chem. Phys.* **2013**, *15*, 13902−13910.
(44) te Velde, G.; Bickelhaupt, F. M.; Baerends, E. J.; Fonseca Guerra, C.; van Gisbergen, S. J. A.; Snijders, J. G.; Ziegler, T. *J. Comput. Chem.* **2001**, *22*, 931−967.
(45) Ciofini, I.; Daul, C. A. *Coord. Chem. Rev.* **2003**, *238*−*239*, 187−209.
(46) Stephens, P. J.; Devlin, F. J.; Chabalowski, C. F.; Frisch, M. J. *J. Phys. Chem.* **1994**, *98*, 11623−11627.
(47) Hessen, B.; Sunshine, S. A.; Siegrist, T.; Jimenez, R. *Mater. Res. Bull.* **1991**, *26*, 85−90.
(48) Garrard, B. J.; Smith, S. H.; Wanklyn, B. M.; Garton, G. *J. Cryst. Growth* **1975**, *29*, 301−304.
(49) Wang, S.; Alekseev, E. V.; Miller, H. M.; Depmeier, W.; Albrecht-Schmitt, T. E. *Inorg. Chem.* **2010**, *49*, 9755−9757.
(50) Woodward, J. D.; Almond, P. M.; Albrecht-Schmitt, T. E. *J. Solid State Chem.* **2004**, *177*, 3971−3976.
(51) Liebau, F. *Structural Chemistry of Silicates: Structure, Bonding, and Classification;* Springer-Verlag: New York, 1985.
(52) Shannon, R. *Acta Crystallogr., Sect. A* **1976**, *32*, 751−767.
(53) Brown, I. D.; Altermatt, D. *Acta Crystallogr., Sect. B* **1985**, *41*, 244−247.
(54) Burns, P. C.; Ewing, R. C.; Hawthorne, F. C. *Can. Mineral.* **1997**, *35*, 1551−1570.

DOI: 10.1021/acs.inorgchem.5b00556
Inorg. Chem. 2015, 54, 5504−5511

(55) Sykora, R. E.; McDaniel, S. M.; Wells, D. M.; Albrecht-Schmitt, T. E. *Inorg. Chem.* **2002**, *41*, 5126−5132.
(56) Sykora, R. E.; Ok, K. M.; Halasyamani, P. S.; Albrecht-Schmitt, T. E. *J. Am. Chem. Soc.* **2002**, *124*, 1951−1957.
(57) Zou, G.; Ye, N.; Huang, L.; Lin, X. *J. Am. Chem. Soc.* **2011**, *133*, 20001−20007.
(58) Gopalakrishnan, J.; Bhat, V.; Raveau, B. *Mater. Res. Bull.* **1987**, *22*, 413−417.
(59) Pagnoux, C.; Verbaere, A.; Kanno, Y.; Piffard, Y.; Tournoux, M. *J. Solid State Chem.* **1992**, *99*, 173−181.
(60) Haile, S. M.; Wuensch, B. J. *Acta Crystallogr., Sect. B* **2000**, *56*, 335−348.
(61) Zou, X.; Dadachov, M. S. *J. Solid State Chem.* **2001**, *156*, 135−142.
(62) Drożdżyński, J. *Coord. Chem. Rev.* **2005**, *249*, 2351−2373.
(63) Mashiyama, H.; Kasano, H.; Yamaguchi, T. *J. Phys. Soc. Jpn.* **1991**, *60*, 45−48.
(64) Jung, J.; Schmitt, G.; Wiehl, L.; Hauser, A.; Knorr, K.; Spiering, H.; Gütlich, P. *Z. Phys. B* **1996**, *100*, 523−534.
(65) Balboni, E.; Burns, P. C. *J. Solid State Chem.* **2014**, *213*, 1−8.
(66) Kindra, D. R.; Evans, W. J. *Chem. Rev.* **2014**, *114*, 8865−8882.
(67) Yeon, J.; Smith, M. D.; Tapp, J.; Möller, A.; zur Loye, H.-C. *J. Am. Chem. Soc.* **2014**, *136*, 3955−3963.
(68) Yeon, J.; Smith, M. D.; Tapp, J.; Möller, A.; zur Loye, H.-C. *Inorg. Chem.* **2014**, *53*, 6289−6298.
(69) Im, W. B.; Fourré, Y.; Brinkley, S.; Sonoda, J.; Nakamura, S.; DenBaars, S. P.; Seshadri, R. *Opt. Express* **2009**, *17*, 22673−22679.
(70) Ramanantoanina, H.; Urland, W.; Cimpoesu, F.; Daul, C. *Phys. Chem. Chem. Phys.* **2014**, *16*, 12282−12290.
(71) Cimpoesu, F.; Dragoe, N.; Ramanantoanina, H.; Urland, W.; Daul, C. *Phys. Chem. Chem. Phys.* **2014**, *16*, 11337−11348.

DOI: 10.1021/acs.inorgchem.5b00556
Inorg. Chem. 2015, 54, 5504−5511